Monthly Notices of the ROYAL ASTRONOMICAL SOCIETY

MNRAS **480,** 1864–1869 (2018)
Advance Access publication 2018 July 19

doi:10.1093/mnras/sty1914

Temperature spectra in the solar wind turbulence

G. Gogoberidze,[1★] Y. M. Voitenko[2] and G. Machabeli[1]

[1] *Institute of Theoretical Physics, Ilia State University, 3 ave. Cholokashvili, Ge0162 Tbilisi, Georgia*
[2] *Solar-Terrestrial Centre of Excellence, Space Physics Division, Belgian Institute for Space Aeronomy, Ringlaan-3-Avenue Circulaire, B-1180 Brussels, Belgium*

Accepted 2018 July 16. Received 2018 June 27; in original form 2017 December 27

ABSTRACT

We study Alfvénic turbulent fluctuations and their spectral properties from MHD to kinetic scales and compare with recent measurements of the *Spektr-R* spacecraft. An apparent contradiction is found between the temperature spectra derived from the *Spektr-R* data and the temperature spectra predicted theoretically. To resolve this contradiction, we show that the temperature fluctuations can be correctly estimated from the *Spektr-R* data only if the mean temperature is isotropic. Since the mean temperature in the solar wind is usually anisotropic, the derived fluctuations appear to be pseudo-temperature rather than temperature. These pseudo-temperature fluctuations are driven by the high-amplitude magnetic fluctuations in Alfvén waves rather than the fluctuations of temperature or thermal velocity. That is why their amplitudes are usually significantly larger than the amplitudes of authentic temperature fluctuations.

Key words: turbulence – solar wind.

1 INTRODUCTION

From early observations of the solar wind, it is known that the energy of plasma fluctuations is mainly concentrated in Alfvén waves (Belcher & Davis 1971) and therefore is stored in perpendicular (with respect to the mean magnetic field $\mathbf{B}_0$) components of the fluctuating velocity and magnetic field. Although compressive waves possess much lower energy, their associated perturbations of density, temperature, and magnetic field strength are also observed in the solar wind for a long time (Intriligator & Wolfe 1970; Goldsein & Siscoe 1972; Bavassano et al. 1982; Grappin, Mangeney & Marsch 1990; Tu et al. 1991; Tu & Marsch 1995; Bruno & Carbone 2013).

Plasma ion moments (density, velocity, and temperature) in the solar wind are usually derived using in situ data collected by means of Faraday cups (Vasylinuas 1971) onboard spacecraft. Although Faraday cups are quite simple devices, derivation of the plasma moments based on the currents measured by the Faraday cups is non-trivial and requires some kind of non-linear fitting technique (Ogilvie 1995; Zastenker et al. 2000; Kasper, Lazarus & Gary 2002; Safrankova et al. 2013b) and some assumptions about particle distribution functions (e.g. Maxwellian or be-Maxwellian distribution function). Because of the complex fitting procedures, determination of the measurement errors in the obtained plasma moments is also non-trivial (Kasper et al. 2006; Gogoberidze et al. 2012).

Recently, Safrankova et al. (2013a, 2016) analysed spectra of velocity, density, and thermal speed in the frequency range 0.001–2 Hz (therefore covering both MHD and kinetic ranges). These spectra were obtained using measurements of the Bright Monitor of the Solar Wind on board the *Spektr-R* spacecraft. The authors found that the spectral indices and spectral breaks between MHD and kinetic ranges were very similar for the bulk velocity and thermal speed, whereas the spectral behaviour of the density fluctuations was entirely different. We found these results surprising because velocity perturbations are mostly due to the dominant Alfvénic component of the turbulence, whereas the density and temperature fluctuations belong to the sub-dominant compressible fraction. This means it is natural to expect similar behaviour of the temperature and density spectra rather than temperature and velocity.

In this paper, we attempt to understand this contradiction by analysing dynamics of high-frequency perturbations in the solar wind and methods of their measurements by *Spektr-R*. We show that some plasma parameters derived from the Faraday cup data can be strongly affected by the anisotropy of the proton distribution function. In particular, the derived thermal velocity is strongly dominated by perturbations of the magnetic field (and not parallel and/or perpendicular proton temperatures) and therefore the observed high frequency spectrum of the thermal speed is mainly produced by the incompressible part of the magnetic field perturbations, thus explaining its similarity with the proton velocity spectrum.

The paper is organized as follows. Polarization relations for Alfvén waves in general form applicable to both magnetohydrodynamic and kinetic scales are presented in Section 2. Spectrum of satellite sampling velocity is derived in Section 3. Density and temperature spectra are studied in Section 4. Methods used for derivation of temperature from the Faraday cup current measure-

★ E-mail: grigol_gogoberidze@iliauni.edu.ge

ments are analysed in Section 5. Discussion and conclusions are given in Section 6.

2 PLASMA MODEL AND POLARIZATION RELATIONS

We study Alfvénic turbulence in the quasi-neutral electron–ion plasma using the two-fluid plasma model. For the waves, we introduce a local reference system associated with every particular wave vector $\mathbf{k}$, where three orthogonal unit vectors are $\mathbf{x} = \mathbf{k}_\perp/k_\perp$; $\mathbf{y} = \mathbf{k}_\perp \times \hat{\mathbf{z}}/k_\perp$; and $\mathbf{z}$ is parallel to the background magnetic field $\mathbf{B}_0$. We assume strong, i.e. critical-balanced turbulence (Goldreich & Sridhar 1995), where the wave periods and characteristic timescales of non-linear interactions are similar. In such turbulence, the Alfvén effect is still strong enough to support the linear wave dispersion and polarization properties, in which case all fluctuating quantities at any wave vector $\mathbf{k}$ can be expressed in terms of the dominant magnetic component B_{ky}. Thus, the components of the ion velocity $\mathbf{v}_k$ and number density n_k are Zhao et al. (2014)

$$v_{kx} = isV_\mathrm{A}\frac{V_\mathrm{A}k_z}{\omega_{ci}}\frac{B_{ky}}{B_0}, \tag{1}$$

$$v_{ky} = -sV_\mathrm{A}\frac{1}{K}\frac{B_{ky}}{B_0}, \tag{2}$$

$$v_{kz} = iV_\mathrm{T}\frac{\rho_\mathrm{T}k_\perp}{K^2}\frac{B_{ky}}{B_0}, \tag{3}$$

$$n_k = isn_0\frac{V_\mathrm{A}k_\perp}{\omega_{ci}K}\frac{B_{ky}}{B_0}. \tag{4}$$

Here, $K \equiv \sqrt{1+\rho_T^2k_\perp^2}$, $\rho_T^2 = (1+T_\mathrm{e}/T_\mathrm{i})\,\rho_i^2$, ρ_i is the ion gyroradius, n_0 is the background number density, ω_{ci} is the ion gyrofrequency, $\mathbf{V}_A = \mathbf{B}_0/\sqrt{4\pi m_\mathrm{p}n_0}$ is the Alfvén velocity, m_p is the proton mass, T_e and T_i are electron and ion temperatures, and $s = k_z/|k_z|$ denotes the wave propagating along ($s = 1$) or against ($s = -1$) background magnetic field $\mathbf{B}_0$.

2.1 Spectrum of the sampling velocity

The sampling frequency $\omega_\mathrm{s} = k_\mathrm{s}V_\mathrm{SW}$ is defined by the sampling wave number

$$k_\mathrm{s} = k_\perp\cos\varphi\sin\chi + k_z\cos\chi, \tag{5}$$

where χ is the sampling angle (angle between $\mathbf{B}_0$ and the solar wind velocity $\mathbf{V}_\mathrm{SW}$), and φ is the azimuthal wave number angle between $\mathbf{k}_\perp$ and ($\mathbf{B}_0$–$\mathbf{V}_\mathrm{SW}$) plane. It is obvious that many Fourier harmonics $\mathbf{k}$ contribute to the same k_s.

If $k_\perp \gg k_z$, as is the case in critical-balanced Alfvénic turbulence, and θ is not close to zero, then

$$k_\mathrm{s} \approx k_\perp\cos\varphi\sin\chi, \tag{6}$$

and all harmonics with

$$k_\perp = \frac{k_\mathrm{s}}{\cos\varphi\sin\chi}. \tag{7}$$

from ∞ to $k_{\perp\mathrm{min}} = k_\mathrm{s}/\sin\theta$ contribute to the sampling wave number k_s. Furthermore, since the amplitudes of perturbations decrease with increasing $k_\perp$, it is usually assumed that the perturbations at k_s are dominated by the perturbations at minimal $k_{\perp\mathrm{min}}$ achieved at $\varphi = 0$. However, we will see below that this is not the case for the perturbations aligned with the sampling direction.

Projections of the ion velocity components v_{kx}, v_{ky}, and v_{kz} upon the sampling direction are

$$v_{s1} = v_{kx}\cos\varphi\sin\chi;$$
$$v_{s2} = v_{ky}\sin\varphi\sin\chi;$$
$$v_{s3} = v_{kz}\cos\chi.$$

For Alfvénic fluctuations, the shear component v_{ky} is largest and defines the sampling velocity fluctuations

$$v_s \approx v_{s2} = v_{ky}\sin\varphi\sin\chi. \tag{8}$$

It is obvious from this expression that the contribution of the dominant Alfvénic component v_{ky} to v_s is missed at $\varphi = 0$. Now, we have to find $k_\perp$ that makes v_s largest. Assume a symmetric azimuthal distribution of fluctuations and the power-law scaling for the amplitudes, $v_{ky} = v_{0y}(k_\perp/k_0)^p$, where k_0 and v_{0y} are the injection scale and amplitude. Then, excluding $\cos\varphi$ from (8) by means of (6), we obtain

$$v_\mathrm{s} = v_{ky}\sin\varphi\sin\chi = v_{ky}\sqrt{1-\cos^2\varphi}\sin\chi$$
$$= v_{0y}\left(\frac{k_\mathrm{s}}{k_0}\right)^p\left[\left(\frac{k_\perp}{k_\mathrm{s}}\right)^p\sqrt{1-\frac{1}{\sin^2\chi}\left(\frac{k_\perp}{k_s}\right)^{-2}}\right]\sin\theta.$$

The maximum contribution to k_s can be found by maximizing this expression with respect to $k_\perp/k_\mathrm{s}$. The corresponding maximum gives the following level of the sampling velocity spectrum:

$$v_\mathrm{s} = v_{0y}\sin^{1-p}\chi\frac{1}{\sqrt{(-p)^p\,(1-p)^{1-p}}}\left(\frac{k_\mathrm{s}}{k_0}\right)^p. \tag{9}$$

This maximum is dominated by the following wavenumber $k_\perp$:

$$\frac{k_\perp}{k_\mathrm{s}} = \frac{1}{\sin\theta}\sqrt{\frac{p-1}{p}}. \tag{10}$$

2.2 Asymptotic MHD range

In the MHD range, $p = -1/3$, then

$$v_\mathrm{s} \approx 0.7v_{0y}\sin^{4/3}\theta\left(\frac{k_\mathrm{s}}{k_0}\right)^{-1/3}. \tag{11}$$

The corresponding power spectrum P_vs has the standard Kolmogorov scaling

$$P_\mathrm{vs} = \frac{v_\mathrm{s}^2}{k_\mathrm{s}} \sim k_\mathrm{s}^{-5/3}. \tag{12}$$

2.3 Asymptotic kinetic range

In the kinetic range, $K \approx \rho_\mathrm{T}k_\perp$, and (2) yields the velocity amplitude scaling

$$v_{ky} \sim \frac{B_{ky}}{k_\perp} \sim \frac{k_\perp^{-2/3}}{k_\perp} \sim k_\perp^{-5/3}. \tag{13}$$

The corresponding power spectrum

$$P_\mathrm{vs} \sim P_{vy} \sim \frac{v_{ky}^2}{k_\perp} \sim k_\perp^{-13/3}. \tag{14}$$

2.4 Density and temperature spectra

At large MHD scales, Alfvén waves themselves are virtually incompressive, and the density perturbations are mainly due to the slow

and/or entropy modes that are passively mixed by the Alfvénic cascade (Lithwick & Goldreich 2003). Therefore, in the MHD range, the density fluctuations n_k^S associated with the slow and entropy modes are expected to have the same anisotropic Kolmogorov spectrum as the magnetic fluctuations of the dominant Alfvénic turbulence:

$$P_n^S \sim k_\perp^{-5/3}. \tag{15}$$

This density spectrum dominates in the asymptotic MHD range $\rho_T^2 k_\perp^2 \ll 1$.

On the other hand, from the linear polarization relation of Alfvén waves

$$\frac{n_k^A}{n_0} = is\frac{V_A k_\perp}{\omega_{ci} K}\frac{B_k}{B_0}, \tag{16}$$

we obtain

$$P_n^A \sim \frac{\left(n_k^A\right)^2}{k_\perp} \sim \frac{k_\perp^2}{1+\rho_T^2 k_\perp^2}\frac{B_{ky}^2}{k_\perp} \tag{17}$$

for the density spectrum associated with Alfvén waves. In the MHD range $\rho_T^2 k_\perp^2 < 1$, the Alfvénic density spectrum (17) increases with $k_\perp$ as $P_n^A \sim k_\perp^{1/3}$ until it reaches a maximum at $\rho_T k_\perp \approx 0.45$. When approaching this wavenumber, the rising Alfvénic density spectrum $P_n^A \sim k_\perp^{1/3}$ partially or fully compensate the MHD-like slope $-5/3$ of the slow/entropy density spectrum. Superposition of the sound density spectrum $\sim k_\perp^{-5/3}$ and Alfvénic density spectrum (17) results in the composite spectra that are significantly flatter than $-5/3$ and can even have a positive slope.

In the strongly dispersive range $\rho_T k_\perp \gg 1$, we have the power-law spectrum

$$P_n^A \sim k_\perp^{-7/3}, \tag{18}$$

that coincides with the magnetic spectrum

$$P_B \sim k_\perp^{-7/3}. \tag{19}$$

Therefore, if the slow and entropy modes are not entirely absent for very low frequencies, then the density spectrum is expected to have two break points and relatively flat plateau between them. A similar interpretation has been proposed by Chandran et al. (2009).

MHD Alfvén waves do not perturb temperature whereas kinetic Alfvén waves are compressible and can produce non-zero perturbation of the ion temperature. In the adiabatic approximation for the ions, the ion temperature spectrum P_T produced by kinetic Alfvén waves is expected to behave similarly to their density spectrum,

$$P_T^A \sim P_n^A. \tag{20}$$

This means that for derivation of the theoretical prediction for the ion temperature spectrum, or equivalently the ion thermal speed spectrum, it is possible to use the same reasoning as for the density spectrum.

3 THERMAL SPECTRA FROM MHD TO KINETIC SCALES

Recent high-frequency (up to 0.032 ms cadence) observations obtained using measurements of the Bright Monitor of the Solar Wind on board the *Spektr-R* spacecraft allowed to derive spectra of the solar wind plasma moments not only in the inertial but also in the kinetic range (Safrankova et al. 2013a, 2016). In the inertial range, obtained spectra of the solar wind velocity and density perturbations are in good agreement with the theoretical predictions presented in the previous section. On the contrary, the spectrum of thermal speed behaves very differently from the theoretical prediction and is much more similar to the solar wind velocity spectrum rather than to the density spectrum as suggested by equation (20). Namely, the thermal speed spectrum has one break point and its spectral index in the inertial interval and position of the spectral break are very close to those of the bulk velocity spectrum. This coincidence seems even more surprising in view of the fact that the velocity spectrum in the asymptotic inertial range is strongly dominated by MHD Alfvén waves which do not have temperature perturbations. Explanation of the non-thermal nature of the 'thermal speed' spectra observed by *Spektr-R* and resolution of the above inconsistency between theory and observations, which are presented in this section, constitute our main results.

For the proton velocity distribution $f(\vec{v})$ the current dI measured by the Faraday cup due to an elementary volume d^3v in the velocity space is (Kasper et al. 2002)

$$\mathrm{d}I = eAf(\vec{v})\hat{n}\cdot\vec{v}\mathrm{d}^3v. \tag{21}$$

Here, A is the effective area of the faraday cup and $\hat{n}$ is the direction along the main axes of the cylinder. As it is long known [e.g. Kasper et al. (2002) and references therein] particle distribution function of protons in the solar wind is not isotropic and can be fitted by bi-Maxwelian distribution with different temperatures along and perpendicular to the mean magnetic field. The total Faraday cup current ΔI due to the bi-Maxwelian distribution can be calculated by integrating equation (21) over all proton velocities perpendicular to $\hat{n}$ and within some speed window along the line of sight. As showed by Kasper et al. (2002), the current ΔI measured by the Faraday cup depends not on the parallel ($T_\parallel$) and perpendicular ($T_\perp$) temperatures, but only on their linear combination

$$T_n = T_\parallel\left(\hat{n}\cdot\hat{b}\right)^2 + T_\perp\left[1-\left(\hat{n}\cdot\hat{b}\right)^2\right]. \tag{22}$$

Here, $\hat{b}$ is the unit vector in the direction of the magnetic field.

One can derive the the proton distribution function moments (density, velocity, parallel, and perpendicular temperatures) using a fitting procedure for the current measurements ΔI either of different Faraday cups [as in the case of very high-resolution data of *Spektr-R* (Zastenker et al. 2000; Safrankova et al. 2016)] or of the same Faraday cups in different speed intervals (Kasper et al. 2002). From the above consideration, it is clear that if the proton distribution function is assumed isotropic, then the corresponding isotropic temperature in both fitting algorithms will be given by the weighted sum of parallel and perpendicular temperatures (22). This is exactly the case with the *Spectr-R* data. Indeed, the algorithm of derivation of the solar wind plasma parameters with extremely high resolution (32 ms) (Zastenker et al. 2000; Safrankova et al. 2016) implies using the simultaneous measurements of six Faraday cups to fit five plasma parameters: three components of the particle flux, flow speed and temperature. However, this method works fine only in the case of isotropic temperature $T_\parallel = T_\perp$. In the case of anisotropic temperature, $T_\parallel$ and $T_\perp$ separately cannot by found, only their linear combination T_n is accessible.

3.1 Thermal and pseudo-thermal spectra

Let us introduce the angle θ between the total magnetic field **B** and $\hat{n}$, such that the measured temperature T_n (22) can be presented as

$$T_n = \left(T_\parallel - T_\perp\right)\cos^2\theta + T_\perp. \tag{23}$$

Furthermore, we will distinguish the mean and fluctuating parts of anisotropic temperatures $T_{\parallel,\perp}$ and magnetic field $\mathbf{B}$:

$$T_\parallel = T_{0\parallel} + \delta T_\parallel; \quad T_\perp = T_{0\perp} + \delta T_\perp;$$

$$\mathbf{B} = \mathbf{B}_0 + \delta\mathbf{B} = \mathbf{B}_0 + \delta\mathbf{B}_\parallel + \delta\mathbf{B}_\perp.$$

Then, $\cos\theta$ can be expressed in terms of fluctuating magnetic fields exactly,

$$\cos\theta = \sqrt{1 - \left(\frac{\delta B_\perp}{B}\right)^2}\cos\theta_0 + \frac{\delta B_\perp}{B}\cos\phi\sin\theta_0, \tag{24}$$

where θ_0 is the angle between the mean magnetic field $\mathbf{B}_0$ and $\hat{n}$, ϕ is the angle between $\delta\mathbf{B}_\perp$ and $(\hat{n}, \mathbf{B}_0)$ plane, and $B = |\mathbf{B}|$,

$$B = \sqrt{B_0^2 + 2B_0\delta B_\parallel + \left(\delta B_\parallel\right)^2 + (\delta B_\perp)^2}.$$

Note that $\cos\theta$ does not depend on $\delta B_\parallel$ if $\delta B_\perp = 0$.

In general, as follows from (23) and (24), fluctuations of T_n are caused by the fluctuations of all involved parameters: $\delta T_\parallel, \delta T_\perp, \delta B_\parallel$, and $\delta B_\perp$. Therefore, the measured spectrum of T_n, or thermal velocity $\sim\sqrt{T_n}$ used by Safrankova et al. (2016), contains contributions of all these sources.

In what follows we show that, for the typical solar wind parameters, the dominant contribution to the spectra of T_n and $\sqrt{T_n}$ comes from the magnetic fluctuations rather than the fluctuations of parallel and perpendicular temperatures. First, we present

$$\cos^2\theta = \cos^2\theta_0 + \delta\left(\cos^2\theta\right), \tag{25}$$

where the $\delta\mathbf{B}$-dependent fluctuating part

$$\delta\left(\cos^2\theta\right) = \left((\cos\phi\sin\theta_0)^2 - \cos^2\theta_0\right)\left(\frac{\delta B_\perp}{B}\right)^2 + \sin(2\theta_0)\cos\phi\sqrt{1 - \left(\frac{\delta B_\perp}{B}\right)^2}\frac{\delta B_\perp}{B}. \tag{26}$$

All above expressions (23)–(26) are quite general, valid for any values of fluctuating parameters. To simplify further analysis, we consider the limit of small perturbations, $\delta B_\perp/B, \delta T/T \ll 1$. Although this condition is not always satisfied for low-frequency magnetic field perturbations (Bruno & Carbone 2013) it is always valid for the high-frequency perturbations close to the spectral break between MHD and kinetic ranges. Then, using (26) in (23) and retaining only leading terms with respect to the small parameters $\delta B_\perp/B, \delta T/T \ll 1$, the fluctuating part of (23) can be simplified to

$$\frac{\delta T_n}{T_{0\perp}} = \cos^2\theta_0\frac{\delta T_\parallel}{T_{0\perp}} + \sin^2\theta_0\frac{\delta T_\perp}{T_{0\perp}} + \left(\frac{T_{0\parallel}}{T_{0\perp}} - 1\right)\sin(2\theta_0)\cos\phi\frac{\delta B_\perp}{B_0}.$$

The dimensionless spectral power of T_n perturbations is thus

$$\frac{\langle\delta T_n^2\rangle}{T_{0\perp}^2} = \frac{\langle\delta T_n^2\rangle_T}{T_{0\perp}^2} + \frac{\langle\delta T_n^2\rangle_B}{T_{0\perp}^2}, \tag{27}$$

where we introduce the thermal contribution

$$\frac{\langle\delta T_n^2\rangle_T}{T_{0\perp}^2} = \left\langle\left(\cos^2\theta_0\frac{\delta T_\parallel}{T_{0\perp}} + \sin^2\theta_0\frac{\delta T_\perp}{T_{0\perp}}\right)^2\right\rangle \tag{28}$$

and the pseudo-thermal contribution due to magnetic fluctuations

$$\frac{\langle\delta T_n^2\rangle_B}{T_{0\perp}^2} = \frac{1}{2}\left(\frac{T_{0\parallel}}{T_{0\perp}} - 1\right)^2\sin^2(2\theta_0)\frac{\langle\delta B_\perp^2\rangle}{B_0^2}. \tag{29}$$

Here, $\langle ...\rangle$ is the ensemble average and we assume that the turbulence is symmetric with respect to ϕ: $\langle\cos\phi\rangle = 0$; $\langle\cos^2\phi\rangle = 1/2$.

The spectral power density of the 'thermal velocity' $V_{Tn} = \sqrt{V_{T\parallel}^2\cos^2\theta + V_{T\perp}^2\sin^2\theta}$ can be found similarly. Again, it consists of two parts, thermal

$$\frac{\langle|\delta V_{Tn}|^2\rangle_T}{V_{T0\perp}^2} = \frac{1}{4}\frac{\cos^2\theta_0\delta\left(V_{T\parallel}^2\right) + \sin^2\theta_0\delta\left(V_{T\perp}^2\right)}{V_{T0\perp}^2} \tag{30}$$

and pseudo-thermal (due to magnetic fluctuations)

$$\frac{\langle|\delta V_{Tn}|^2\rangle_B}{V_{T0\perp}^2} = \frac{1}{8}\frac{\left(T_{0\parallel}/T_{0\perp} - 1\right)^2\sin^2(2\theta_0)}{\left(T_{0\parallel}/T_{0\perp} - 1\right)\cos^2\theta_0 + 1}\frac{\langle\delta B_\perp^2\rangle}{B_0^2}. \tag{31}$$

It is long known that in the inertial interval of the solar wind turbulence the dimensionless magnetic fluctuations $\delta B_\perp/B_0$ associated with incompressible Alfvén waves are about 1 order of magnitude higher than the amplitudes of compressional fluctuations associated with perturbations of density and/or temperature, $\sim\delta T_{\parallel,\perp}/T_{0\perp}$ (Goldsein & Siscoe 1972; Grappin et al. 1990; Tu et al. 1991; Tu & Marsch 1995):

$$\frac{\delta B_\perp}{B_0} \gg \frac{\delta T_\parallel}{T_{0\perp}}, \frac{\delta T_\perp}{T_{0\perp}}.$$

Then from (29) it is seen that, excluding specific cases when $\sin 2\theta_0 \leq 0.1$ or $|T_{0\parallel}/T_{0\perp} - 1| \leq 0.1$, the measured power spectra of T_n (as well as the corresponding power spectra of V_{Tn}) are dominated by the Alfvénic magnetic fluctuations rather than the fluctuations of the temperature itself.

To estimate the maximum of the thermal contribution (the first term in the rhs of equation 27), we assume that at any time-scale τ the perturbations $\delta T_\perp(\tau)$ and $\delta T_\parallel(\tau)$ are equal $\delta T_\perp = \delta T_\parallel = \delta T$ and perfectly correlated. In this case, after averaging the thermal contribution in the dimensionless rms power of perturbations is

$$\frac{\langle\delta T_n^2\rangle_T}{T_{0\perp}^2} \approx \frac{\langle\delta T^2\rangle}{T_{0\perp}^2}. \tag{32}$$

Now, we estimate the magnetic contribution to the observed spectrum. As follows from equation (29), this contribution vanishes if $T_{0\parallel} = T_{0\perp}$ or $\sin 2\theta_0 = 0$. Although in the slow solar wind there are intervals with $T_{0\parallel} \approx T_{0\perp}$ (Hellinger et al. 2006), usually difference between parallel and perpendicular temperatures is quite significant. Taking as the typical values $\sin^2 2\theta_0 \sim \left|\frac{T_{0\parallel}}{T_{0\perp}} - 1\right| \sim 0.5$ (Kasper et al. 2006), contribution of the Alfvén waves (29) reduces to

$$\frac{\langle\delta T_n^2\rangle_B}{T_{0\perp}^2} \approx \frac{1}{8}\frac{\langle\delta B_\perp^2\rangle}{B_0^2}. \tag{33}$$

Estimations indicate that the ratio of dimensionless rms amplitudes $\lambda = (\delta T^2/T^2)/(\delta B_\perp^2/B_0^2)$ in the inertial range of stationary solar wind sub-intervals is usually of the order 10^{-2} and almost never exceeds 10 per cent even in the slow streams of the solar wind, which are known to be much more compressible compared to perturbations in the fast solar wind (Bruno & Carbone 2013).

An illustrative example for a stationary stream is given in Fig. 1. Solid line shows dependence of the ratio of dimensionless rms amplitudes $\lambda(\tau) = (\delta T(\tau)^2/T_0^2)/(\delta B_\perp(\tau)^2/B_0^2)$ as a function of time-scale τ for a stationary stream of the slow solar wind. We use data obtained by the WIND spacecraft at 3 s resolution. Magnetic field data is provided by the MFI instrument (Lepping et al. 1995) and density and velocity data by the 3DP instrument (Lin et al. 1995) measured during a stationary slow stream. The start time of the interval is 12:00 2000 April 4 and stop time is 16:00 of 2000 April 6. During this interval the solar wind speed remained about 300 km s^{-1}. As it is seen from Fig. 1, $\lambda < 0.03$ except for very small τ.

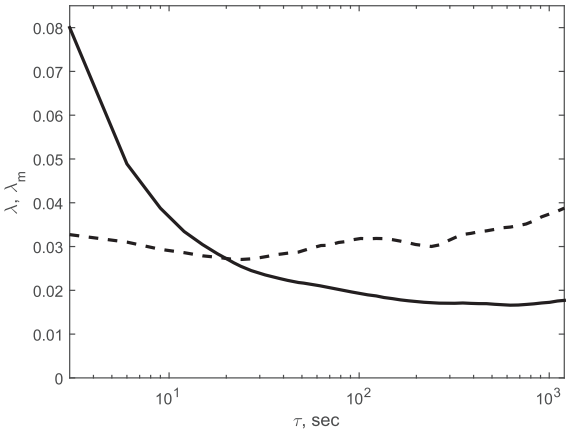

Figure 1. The ratio of dimensionless rms amplitudes $\lambda(\tau) = (\delta T(\tau)^2/T^2)/(\delta B_\perp(\tau)^2/B_0^2)$ (solid line) and $\lambda_m = \delta\,|\mathbf{B}(\tau)|^2/\delta B_\perp(\tau)^2$ (dashed line, see the text for details) as a function of time-scale τ for a stationary stream of the slow solar wind.

We suggest that this enhancement at the small scales is probably due to measurement uncertainties (which are known strongly affecting plasma parameters at high frequencies Kasper et al. 2006; Gogoberidze et al. 2012) rather than indicating a real enhancement of compressible perturbations. To support this suggestion, we present another important characteristic of compressible/non-Alfvénic perturbations (Tu & Marsch 1995; Bruno & Carbone 2013) $\lambda_{\rm m} = \delta\,|\mathbf{B}(\tau)|^2/\delta B_\perp^2(\tau)$ by dashed line in Fig. 1. As can be seen $\lambda_{\rm m}$ is approximately constant and does not increase with decreasing time-scale.

The above consideration suggests that the thermal-speed spectra reported by Safrankova et al. (2016) are in fact the pseudo-thermal spectra dominated by the magnetic fluctuations rather than the temperature fluctuations. This conclusion is supported by the fact that the level of spectra reported by Safrankova et al. (2016) cannot be caused lonely by the temperature fluctuations. Indeed, the spectrum of the (pseudo-)thermal speed in their fig. 1(b) is only about three times lower than the spectrum of the bulk speed driven by Alfvén waves (their fig. 1a), whereas the authentic temperature fluctuations should be at least one order less energetic (Goldsein & Siscoe 1972; Tu et al. 1991; Tu & Marsch 1995).

To be more specific, let us utilize the straightforward expression

$$\frac{\langle \delta V_{Bn}^2\rangle}{V_{\rm A}^2} = \langle \cos^2\phi\rangle \sin^2\theta_0 \frac{\langle \delta V_\perp^2\rangle}{V_{\rm A}^2} = \frac{1}{2}\sin^2\theta_0 \frac{\langle \delta B_\perp^2\rangle}{B_0^2} \tag{34}$$

relating the bulk velocity fluctuations δV_{Bn} measured by Safrankova et al. (2016) and magnetic fluctuations due to Alfvén waves. By means of (34), we can eliminate $\langle \delta B_\perp^2\rangle$ from (31) thus arriving to the following estimation for the velocity spectra ratio:

$$\frac{\langle |\delta V_{Tn}|^2\rangle_B}{\langle \delta V_{Bn}^2\rangle} = \frac{\left(T_{0\parallel}/T_{0\perp} - 1\right)^2 \cos^2\theta_0}{\left(T_{0\parallel}/T_{0\perp} - 1\right)\cos^2\theta_0 + 1}\,\frac{V_{\rm T\perp}^2}{V_{\rm A}^2}. \tag{35}$$

With reasonable values $T_{0\parallel}/T_{0\perp} \sim 0.5$ or $T_{0\parallel}/T_{0\perp} \sim 1.8$ and $V_{T\perp}^2/V_A^2 \lesssim 1$, (35) easily explains the modest ratio $\gtrsim 1/3$ between $\langle |\delta V_{Tn}|^2\rangle_B$ and $\langle \delta V_{Bn}^2\rangle$ deduced from figs 1(a) and (b) by Safrankova et al. (2016). With autentic temperature perturbations this ratio would be at least one order less (Goldsein & Siscoe 1972; Tu et al. 1991; Tu & Marsch 1995).

4 DISCUSSION AND CONCLUSIONS

We have shown that the nature of 'temperature fluctuations' derived from the currents of Faraday cup(s) is strongly affected by the temperature anisotropy. If the temperature anisotropy is close to zero, then the derived 'temperature fluctuations' are dominated by the perturbations of real temperature (thermal speed). However, when the temperature anisotropy is finite, as is typical for the solar wind, the 'temperature fluctuations' change their source and nature being driven by the Alfvénic magnetic fluctuations rather than the fluctuating parallel and/or perpendicular temperatures. Such 'temperature fluctuations', presented by (29) and (31), we call pseudo-thermal. The pseudo-thermal fluctuations and the bulk speed fluctuations have the common source, Alfvén waves, which explains a close similarity of their spectra.

The pseudo-thermal spectra should be even more similar (but with different amplitudes) to the magnetic spectra with which they share the same source – Alfvénic magnetic fluctuations. Therefore, as the magnetometer onboard *Spektr-R* is not operational (Safrankova et al. 2013a) and in situ magnetic spectra are not available, a good proxy for them can be provided by the pseudo-thermal spectra. These spectra may be useful for testing some theoretical predictions even in the absence of magnetic data. Below we summarise several preliminary results in this direction.

(1) Apparent fluctuations of the proton thermal velocity and the corresponding spectra deduced from the *Spektr-R* data are largely due to the Alfvénic magnetic fluctuations rather than the temperature fluctuations. Fluctuations of the bulk velocity and their spectra, observed simultaneously by *Spektr-R*, are produced by the Alfvénic velocity fluctuations. These two facts, together with the Alfvénic link (2) between velocity and magnetic fluctuations, probably explain why the pseudo-thermal velocity spectra are so similar to the bulk velocity spectra.

(2) The relative power of the pseudo-thermal and bulk velocity spectra is presented by (35). Using spectra measured by *Spektr-R* in this relation, one can deduce two plasma parameters, temperature anisotropy $|T_{0\parallel}/T_{0\perp} - 1|$ and plasma $\beta_\perp = (V_{T\perp}/V_A)^2$. By coincidence, (35) can be re-written in the form proportional to the quantity $|\beta_\parallel - \beta_\perp|$, sufficient value of which is essential for development of firehose instability at $\beta_\parallel > \beta_\perp$, or mirror instability at $\beta_\parallel < \beta_\perp$ (Hellinger et al. 2006).

(3) We argued that the authentic thermal spectrum in the solar-wind turbulence (28) should closely resemble the density spectrum shown in fig. 1(c) by Safrankova et al. (2016). However, this thermal spectrum is usually obscured by the magnetic pseudo-thermal spectrum (the last term in 27), and can rarely rise above it. As follows from equation (29), careful selection of the intervals with $T_{0\parallel} = T_{0\perp}$ or $\sin 2\theta_0 \approx 0$ could help in extracting authentic thermal spectra from the *Spektr-R* data and compare them with the density spectra.

(4) In view of above, several previous conclusions about similarity between the thermal and bulk velocity spectra (Safrankova et al. 2013a, 2016) appear to be incorrect. The reason behind these mistakes is that the authors did not distinguish the proper thermal spectrum from the pseudo-thermal spectrum established by magnetic fluctuations. Between these two, only the latter spectrum can resemble the bulk velocity spectrum. On the contrary, the authentic thermal spectrum should resemble the density spectrum, which is still subject for future experimental verifications.

(5) The average across scales value of the mean spectral index of the bulk speed is -3.1 in the kinetic range (Safrankova et al. 2016), but the slope varies across kinetic scales reaching local values $\lesssim -4$ in agreement with (14). The median pseudo-thermal (magnetic)

spectrum is flatter, its −2.4 slope is in good correspondence to the magnetic slope −7/3 (19) slightly steepened by the damping and intermittency.

ACKNOWLEDGEMENTS

This work has been supported by Shota Rustaveli National Science Foundation grants FR/51/6-300/14 and FR/516/6-300/14.

REFERENCES

Bavassano B., Dobrowolny M., Mariani F., Ness N. F., 1982, JGR, 87, 3617
Belcher J. W., Davis L., 1971, J. Geophys. Res., 76, 3534
Bruno R., Carbone V., 2013, Living Rev. Solar Phys., 10, 2
Chandran B. D. G., Quataert E., Howes G. G., Xia Q., Pongkitiwanichakul P., 2009, ApJ, 707, 1668
Gogoberidze G., Chapman S. C., Hnat B., Dunlop M. W., 2012, MNRAS, 426, 951
Goldreich P., Sridhar S., 1995, ApJ, 438, 763
Goldstein B., Siscoe G. L., 1972, in Sonett C. P., Coleman P. J., Jr, Wilcox J. M., eds, Solar Wind, NASA SP-308. National Aeronautics and Space Administration, Washington, p. 506
Grappin R., Mangeney A., Marsch E., 1990, J. Geophys. Res., 95, 8197
Hellinger P., Travniček P., Kasper J. C., Lazarus A. J., 2006, Geophys. Res. Lett., 33, L09101
Intriligator D. S., Wolfe J. H., 1970, ApJ, 162, L187
Kasper J. C., Lazarus A. J., Gary S. P., 2002, Geophys. Res. Lett., 29, 1839
Kasper J. C., Lazarus A. J., Steinberg J. T., Ogilvie K. W., Szabo A., 2006, J. Geophys. Res., 111, A03105
Lepping R.P. et al., 1995, Space Sci. Rev., 71, 125
Lin R.P. et al., 1995, Space Sci. Rev., 71, 207
Lithwick Y., Goldreich P., 2003, ApJ, 582, 1220
Ogilvie K. W. et al., 1995, Space Sci. Rev. 71, 55
Safrankova J., Nemecek Z., Prech L., Zastenker G. N., 2013a, Phys. Rev. Lett., 110, 025004
Safrankova J. et al., 2013b, Space Sc. Rev., 175, 165
Safrankova J., Nemecek Z., Nemec F., Prech L., Chen C. H. K., Zastenker G. N., 2016, ApJ, 825, 121
Tu C.-Y., Marsch E., 1991, Ann. Geo., 9, 748
Tu C.-Y., Marsch E., 1995, Space Sci. Rev., 73, 1
Vasylinuas V. M., 1971, Deep Space Plasma Measurements, in Methods of Experimental Physics. Academic Press, New York, p. 49
Zastenker G. N. et al., 2000, Cosmic Res., 38, 20
Zhao J. S., Voitenko Y., Yu M. Y., Lu J. Y., Wu D. J., 2014, ApJ, 793, 107

This paper has been typeset from a TEX/LATEX file prepared by the author.